JOURNAL OF OPTOELECTRONICS AND ADVANCED MATERIALS Vol. 12, No. 3, March 2010, p. 773 - 776

High-current pulsed arc synthesis of encapsulated silver nanoparticles: control of the relative size of the metallic nucleus

F. MAYA[a,b*], S. MUHL[b], M. MIKI-YOSHIDA[a]
[a]*Departamento de Microscopía Electrónica, Centro de Investigación en Materiales Avanzados, Miguel de Cervantes 120, Chihuahua, Chih., CP 3110, México*
[b]*Instituto de Investigaciones en Materiales, Universidad Nacional Autónoma de México, México D.F. 04510*

We report the dependence of the radius of the encapsulated nanoparticles, the inner metal nucleus and the thickness of the a-C encapsulant layer on the argon gas pressure and the diameter of the silver electrode in the high-current pulsed arc synthesis technique. The deposits were studied by XRD, TEM, SEM and EDX. The radius of the nanoparticles varied from ~55 to 9 nm as the Argon pressure was decreased from 106 to 13 kPa, at 66 kPa the radius of the nanoparticle and nucleus decreased from 34 to 11 nm and 19 to 9 nm, respectively, as the cross-sectional area of the silver electrode was increased from 0.13 to 1.13 x $10^{-6}m^2$.

(Received June 30, 2009; accepted October 12, 2009)

Keywords: Arc evaporation, High current, Silver nanoparticles

1. Introduction

The discovery of the formation of diverse nanostructured forms of carbon by the Kratschmer-Huffman carbon arc method and the modifications developed by Dravid together generated a strong interest in the production of nanostructured materials for many applications [1,2] Such techniques have been used to produce not only carbonaceous materials but also a wide range of encapsulated metal nanoparticles (EMN´s) using DC continuous arcs, of around 100A in He, Ar or H at 26.7 – 66.5 kPa. The interest in core-shell nanostructured materials arises from the fact that their intrinsic properties can be tuned by changing either their relative size [3] or the composition of both core and shell [4]. For example, both nanoshells (a dielectric core surrounded by a metallic shell) and nanocables (nanowires encapsuled in various kind of nanotubes) have been widely investigated recently [5-8].

One of the more interesting of such core-shell systems is that of Ag nanoparticles encapsulated with crystalline or amorphous carbon. Silver exhibits outstanding optical properties and excellent thermal and electrical conductivity and, therefore, has been extensively used in catalysis, electronics, photonics, photography, biological labeling, surface-enhanced Raman scattering and optical devices [9-11]. However, these nanoparticles readily oxidize in air and have a poor biocompatibility; nevertheless, if a carbon outer-shell is added both problems are solved and the range of prospective applications is increased. Based on this strategy, composite nanostructures, Ag/C nanocables and Ag/C nanoparticles, have been prepared by some groups [12-14].

In this work we have used high-current pulsed electric arcs in argon between graphite and silver electrodes to produce silver-carbon nanoparticles.

2. Experiment

The experimental apparatus is described in detail elsewhere [15,16]. We used for electrodes, high purity AERO graphite from ESPI of 3.12 x 10^{-3} m diameter and silver wires (99.9% purity) of different diameters. The temporal form of the arc current was measured by the voltage-drop across a low inductance 0.98 mW resistor using a HP54522A Digital oscilloscope. For the experiments versus pressure, range from 13 to 106 kPa, the arc was generated in argon (99.99 % purity) using an applied voltage of 60V.to the capacitor bank For the experiments with variable diameters of the silver electrode the applied voltage was 40V. For the TEM analysis, the deposit was removed by ultrasonic agitation in methanol. Drops of this liquid were then applied to a TEM grid coated with a holey polymer layer, or for the SEM, EDX and XRD analysis the liquid was applied to a piece of silicon wafer. At least 3 samples were prepared under each of the experimental conditions and the results are an average for each condition.

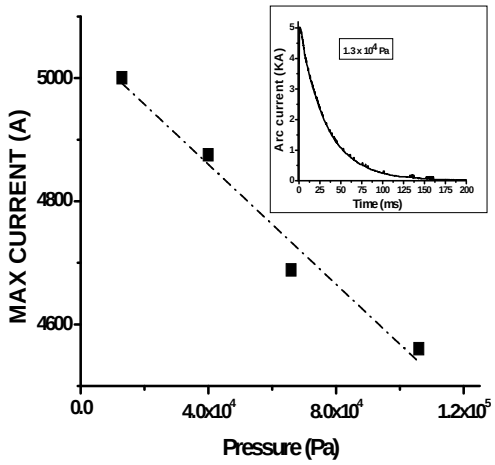

Fig. 1. The measured maximum of the arc current as a function of the argon gas pressure. The inset shows the temporal variation of the arc current for a gas pressure of 13 kPa.

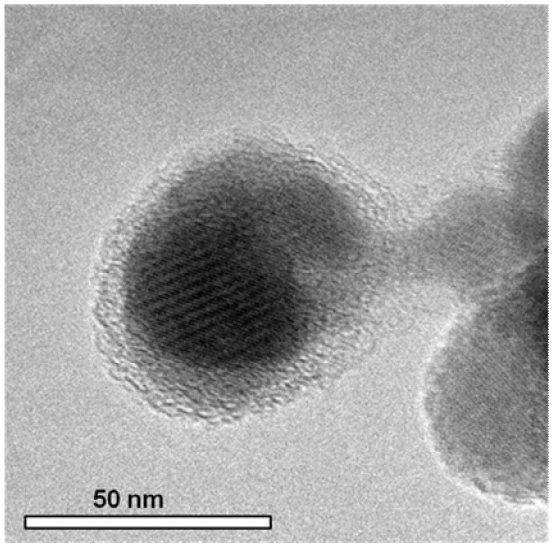

Fig. 2. A TEM micrograph of a silver nanoparticle prepared in 40 kPa of argon.

3. Results

Fig. 1 shows that the maximum arc current decreased linearly as the argon pressure was increased from 13 to 106 kPa. The inset in Fig. 1 shows the temporal variation of the arc current; the FWHM duration of the arc was approximately 25 ms. Fig. 2 is a TEM micrograph of a nanoparticle prepared using an argon pressure of 40 kPa the crystalline silver nucleus and amorphous carbon coat can be clearly seen. More than 20 different sized nanoparticles have been studied by TEM and the carbon layer was always amorphous. The a-C layer was seen to be a very effective chemical barrier since no reaction was observed when nanoparticles were added to concentrated hydrochloric acid.

The left-hand side axis of figure 3 and 4 shows the average particle radius, obtained from the measurements of at least 50 particles in SEM micrographs, of the deposits prepared at the different pressures or at 66kPa for the different silver electrode diameters, respectively. The average composition of the samples was measured over an area which included the 50 nanoparticles, only Ag, C, Si and O were detected and measurement of the silicon substrate without nanoparticles showed that the oxygen signal was from the native SiOx layer.

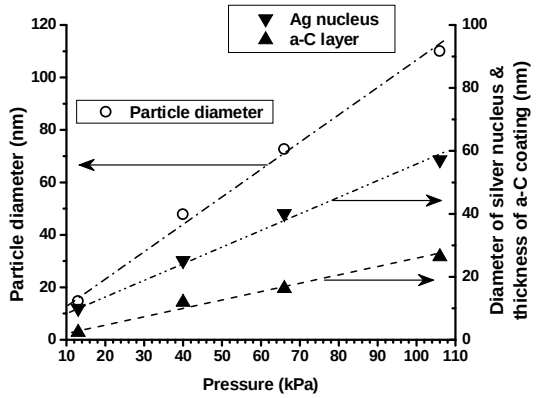

Fig. 3. The left hand side axis shows the measured nanoparticle radius versus the argon gas pressure. The right hand side axis shows the calculated radius of the silver nucleus and the a-C coating.

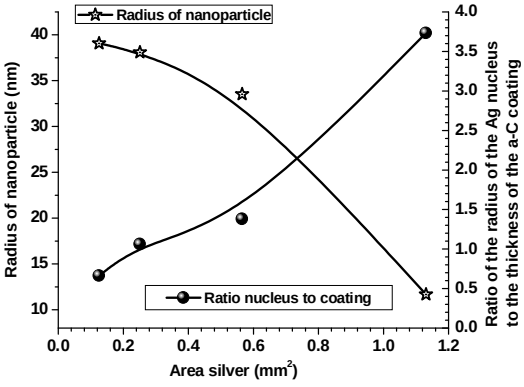

Fig. 4. The left hand side axis shows the measured nanoparticle radius versus the area of the Ag electrode. The right hand side axis shows the calculated radius of the silver nucleus and the a-C coating.

The TEM analysis of the deposits demonstrated that the nanoparticles consist of a small crystalline metal nucleus cover by an amorphous carbon layer, therefore, if we assume that the particle is spherical then:

$$\frac{m_C}{m_{Ag}} = \frac{\rho_C}{\rho_{Ag}} * \frac{r_{np}^3 - r_{Ag}^3}{r_{Ag}^3}$$

where m_C and m_{Ag} are the mass of carbon and silver in the nanoparticle, ρ_C and ρ_{Ag} are the densities of carbon and silver, r_{np} and r_{Ag} are the radii of the nanoparticle and the silver nucleus. This can be rearranged to give:

$$r_{Ag} = \frac{r_{np}}{\sqrt[3]{\frac{m_C}{m_{Ag}} * \frac{\rho_{Ag}}{\rho_C} + 1}}$$

Using the bulk density of silver, 10.5 g/cm^3, and an estimated amorphous carbon density of 1.8 g/cm^3 [17], together with the measured nanoparticle radius and the C to Ag mass ratio of the deposit calculated from the EDX measured composition (ignoring the signal from Si and O), see Table 1, it was possible to estimate the radius of the silver nucleus and the thickness of the a-C layer in the nanoparticle. The variation of the radius of the nucleus and layer thickness with argon gas pressure is plotted in Fig. 3 against the right-hand axis. For the range of pressures studied, the nanoparticle radius, the nucleus radius and the layer thickness increased linearly with the gas pressure ($R \geq 0.98$).

Table 1. The composition of the nanoparticles, expressed as percentage mass of silver and carbon, for the argon pressures and silver electrode diameters used. The radius of the crystalline grains size obtained from the FWHM of the x-ray diffraction peaks and the radius of the silver nucleus of the nanoparticles calculated as described above.

Pressure (kPa)	Area of the Ag electrode (mm^2)	% mass of carbon (m_C)	% mass of silver (m_{Ag})	Ratio of the mass of carbon to silver (m_C/m_{Ag})	Radius of the silver nucleus (nm)	
					XRD	Calculated
13	1.27	32.36	67.64	0.48	10.4	5.0
40	1.27	44.73	55.27	0.81	14.0	10.3
66	1.27	52.02	47.98	1.08	22.6	12.61
106	1.27	57.22	42.78	1.34	46.1	28.5
66	0.13	75.54	24.46	2.52	36.3	15.60
66	0.25	61.96	38.04	1.08	34.8	19.62
66	0.56	41.4	58.6	0.71	29.3	19.44
66	1.13	15.1	84.9	0.18	10.6	9.21

The right-hand axis of Fig. 4 shows the variation of the ratio of the silver nucleus to the thickness of the a-C layer as a function of the area of the silver electrode used. It can be clearly seen that as the electrode area was increased the total radius of the nanoparticle decreased but the relative thickness of the a-C coating was considerable smaller.

The XRD spectrum obtained from all of the deposits only contained diffraction peaks from pure silver; no peaks associated with graphite were observed. The Table 1 lists the grain size obtained by a Scherrer analysis of the silver 111 XRD peaks [18]. The radius of the nucleus obtained from the mass ratio/density analysis, as described above, and the grain size from the XRD data were very similar for the lowest pressures but the XRD value was almost double

that of the mass ratio calculated value for the highest pressures.

4. Discussion

The discrepancies in the radii of the nuclei determined by the two methods are probably related to the group of particles sensed by each technique: the XRD grain size is an average value somewhat weighted towards the larger mass nanoparticles and the SEM images showed that the distribution of sizes was almost proportional to the size of the nanoparticle, the EDX size is based on a somewhat truer average since the compositional information was collected over an area of various square microns. The variation of the nucleus to coating size may be due to the fact that for a thinner silver electrode proportionally less total mass of silver is evaporated during a pulse. This could be because: 1) there is a temperature gradient along the length of the electrode away from the point of contact and/or 2) at a certain length of evaporated silver the plasma is extinguished. However, the possibility 2 did not occur, except at very short times relative to the duration of the pulse, because the arc current measurements rarely showed an interruption of the arc. In the case 1, the amount of energy delivered to the graphite should be almost constant regardless of the area of the silver electrode. Therefore, a possible explanation of the results is that for each pulse the amount of emitted carbon vapour was constant but amount of silver vapour increased as the silver electrode area was increased. The results from the two studies indicate that the diameter of the produced nanoparticles also depends on the arc current used; in the table the nanoparticle radius for 66kPa, an applied voltage of 60V and a silver electrode of 1.27 mm^2 was 72.6 nm and for 66 kPa, an applied voltage of 40 V and a silver electrode of 1.13 mm^2 the size was 23.3 nm.

5. Conclusions

In this work we have produced and characterized encapsulated silver nanoparticles by high-current pulsed electric arcs in an Ar atmosphere. The resulting nanoparticles consist of a crystalline silver nucleus coated with amorphous carbon. It was found that the diameter of the nanoparticles increased when the gas pressure was decreased, and when the area of the silver electrode was decreased or the applied voltage to the capacitor bank (arc current) was increased. The size of the relative silver nucleus and the thickness of the amorphous carbon coating were found to be somewhat dependent on gas pressure and strongly dependent on the area of the silver electrode. The nanoparticles could be collected either as a colloidal suspension and the amorphous carbon coating was an effective chemical barrier.

Acknowledgements

The authors wish to thank Hermilio Zarco for his help with the experimental work.

References

[1] W. Kratschmer, L. D. Lamb, K. Fostiropoulos, D. R. Huffman, Nature **347,** 354 (1990).
[2] J. J. Host, M. J. Teng, B. Elliot, J. Hwang, T. O. Mason, D. L. Johnson, V. P. Dravid, J. Mater. Res. **12,** 1268 (1997).].
[3] O. Peña, U. Pal, L. Rodríguez-Fernández, A. Crespo-Sosa, J. Opt. Soc. Am. B **25**, 1371 (2008).
[4] B. L. Cushing, V. L. Kolesnichenko, C. J. O'Connor, Chem. Rev. **104**, 3893 (2004).
[5] R. D. Averitt, S. L. Westcott, N. J. Halas, J. Opt. Soc. Am. B **16**, 1824 (1999).
[6] A. M. Schwartzberg, T. Y. Olson, Ch.E. Talley, J. Z. Zhang, J. Phys. Chem. B **110**, 19935 (2006).
[7] L. D. Zhang, G. W. Meng, F. Phillipp, Mater. Sci. Eng.: A **286**, 34 (2000).
[8] J. Jang, B. Lim, J. Lee, T. Hyeon, Chem. Commun., 83 (2001).
[9] K. Dai, L. Shi, J. Fang, Y. Zhang, Mater. Sci. Eng.: A **465**, 283 (2007).
[10] T. Oku, T. Kusunose, T. Hirata, N. Sato, R. Hatakeyama, K. Niihara, K. Suganuma, Diamond and Related Materials **9**, 911 (2000).
[11] P. V. Adhyapak, P. Karandikar, K. Vijayamohanan, A. A. Athawale, A. J. Chandwadkar, Mater. Lett. **58**, 1168 (2004).
[12] X. M. Sun, Y.D. Li, Adv. Mater. **17**, 2626 (2005).
[13] L. B. Luo, S. H. Yu, H. S. Qian, T. Zhou, J. Am. Chem. Soc. **127**, 2822 (2005).
[14] V. Rodríguez-Iglesias, O. Peña, H.G. Silva-Pereyra, L. Rodríguez-Fernández, G. Kellermann, J. C. Cheang-Wong, A. Crespo-Sosa, A. Oliver, Appl. Phys. B, in press.
[15] S. Muhl, F. Maya, S. Rodil, E. Camps, M. Villagrán, A. García, Thin Solid Films **433**, 50-56 (2003).
[16] S. Muhl, F. Maya, S. Rodil, G. Gonzalez, E. Camps, L. Escobar-Alarcon, M. Espinosa-Pesqueira, J. Optoelectron. Adv. Mater. **7**, 231-236 (2005).
[17] A. C. Ferrari, A. Libassi, B. K. Tanner, V. Stolojan, J. Yuan, L. M. Brown, S. E. Rodil, B. Kleinsorge, J. Robertson, Phys. Rev. B. **62**, 11089 (2000).
[18] A. L. Patterson, Phys. Rev. **56**, 978 (1939).

*Corresponding author: muhl@servidor.unam.mx